Pickering emulsion as template for porous bioceramics in the perspective of bone regeneration

Karline Pascaud, M. Mercé, Armand Roucher, Mathieu Destribats, Rénal Backov, Véronique Schmitt, Romain Sescousse, F. Brouillet, S. Sarda, Maria-Inês Ré

Pickering emulsion as template for porous bioceramics in the perspective of bone regeneration

K. Pascaud [a,b], M. Mercé [c], A. Roucher [c], M. Destribats [c], R. Backov [c], V. Schmitt [c], R. Sescousse [a], F. Brouillet [d], S. Sarda [b,*], M.I. Ré [a]

[a] *IMT Mines Albi, RAPSODEE UMR CNRS 5302, Albi, France*
[b] *CIRIMAT, INPT-CNRS-UPS, Université de Toulouse, Université Paul Sabatier, Toulouse, France*
[c] *Univ. Bordeaux, CRPP UMR CNRS 5031, Pessac, France*
[d] *CIRIMAT, INPT-CNRS-UPS, Université de Toulouse, Faculté des Sciences Pharmaceutiques, Toulouse, France*

GRAPHICAL ABSTRACT

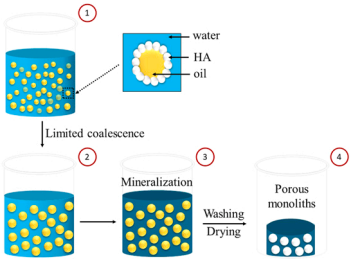

ABSTRACT

Calcium phosphate (CaP) based bioceramics are widely used as bone substitutes. The most encountered CaP ceramics are obtained from high temperature phases. However, their bioactivity and their association with biomolecules are limited, as well as their bioresorption *in-vivo*. The aim of this work is to develop biomimetic low temperature apatites ceramics with tunable porosity *via* biocompatible high internal phase Pickering emulsions. The biocompatible emulsions developed were stabilized by stoichiometric hydroxyapatite (HA) particles. Several parameters (mass of HA particles, oil/water weight ratio, electrolytes concentration in the aqueous phase) were investigated to define the optimized formulation conditions leading to a kinetically stable monodisperse emulsion with a minimum drop diameter of 200 μm and drops enough percolated to induce interconnected porosity. Two types of porous bioceramics were produced by low temperature processes with controlled composition and porosity, evidenced by X-ray microtomography: calcium phosphate monoliths from an apatitic gel, and silica-HA monoliths *via* a sol-gel process. These low temperature processes should provide bioceramics able to perform bioactivity and bio-resorption *in-vivo*, and could prefigure a drug or other therapeutic ions-delivery disposals for filling bone defects in maxillofacial or orthopedic surgery.

Keywords:
Pickering Emulsion
Porous biomaterials
Bioceramics
Hydroxyapatite
Sol-gel process

1. Introduction

The need of bone graft substitutes for dental, craniofacial and orthopedic reconstructions is rapidly increasing due to global population growth and extension of life expectancy (about 2 billion persons up to 65 by 2050) [1]. Among different biomaterials, bioceramics is a large class of biomaterials used in clinical practice for the repair and reconstruction of diseased or damaged parts of the body in various forms including solid pieces, powders, granules, coatings on metal joint prostheses, bone cement or porous scaffolds [2]. Calcium phosphate (CaP) based bioceramics are widely used as bone substitutes due to their biocompatibility and bioactivity.

From a structural point of view, the most encountered CaP ceramics are based on high temperature phases as hydroxyapatite (HA), β-tricalcium phosphates (β-TCP) or α-tricalcium phosphates (α-TCP). Their elaboration processes have been extensively reviewed in literature [3]. However, their bioactivity (osteoblasts stimulation, cells adhesion and proliferation) and their association with biomolecules and/or proteins are limited, as well as their bio-resorption *in-vivo*, due to their low specific surface area and poor chemical reactivity. Another key property for these bioceramics is porosity, indeed pore sizes (> 200 μm), morphology and connectivity strongly affect bone formation (cell distribution/migration and angiogenesis) [4,5]. Several techniques can be used to create porous CaP scaffolds based on high temperature process (> 1000 °C), by combining blowing agents as polymers microspheres with powders or slurries, which burn away from the molding body during sintering [6]. However, the final porosity (shape, pore size distribution, interconnection) is not fully controlled.

Recently, a new process of preparation of porous silica monoliths (which are of a single piece as opposed to powders) *via* high internal Pickering emulsions as porous template at low temperatures (room temperature) was patented [7]. Pickering emulsions are emulsions in which surfactants have been substituted by solid particles [8,9]. Those particles have the benefit of being adsorbed irreversibly onto the oil-water interface, the as-made emulsions are then more stable than the ones employing surfactants as stabilizing agents. A wide variety of particles have been used in the literature to stabilize emulsions, silica being the most extensively employed [10–13]. Multiple parameters have been reported [14] for tuning the emulsion properties while playing with diverse characteristics of the stabilizing particles (size, shape, wettability, surface properties, concentration…). These emulsions are well known for their long-term stability [15,16] because of the high energy necessary to desorb the particles once anchored at the oil-water interfaces.

The aim of this work is to develop biomimetic apatites ceramics with tunable porosity *via* biocompatible high internal phase Pickering emulsions, by employing the low temperature synthesis process previously patented [6,7]. Biomimetic nanocrystalline apatites analogous to bone can be easily obtained by precipitation at low temperature and at physiological pH [17]. They exhibit a high surface reactivity due both to their nanometric size and the existence of a hydrated layer rich in labile environments of mineral ions on the crystal surfaces. Their reactivity and tunable physicochemical characteristics offer decisive advantages for biological applications; moreover, the loosely bound ions of the hydrated layer offer a wide range of reaction possibilities from ion exchange to adsorption of biologically interesting molecules (drugs, growth factors) which have been poorly exploited with porous bioceramics [17–19].

The emulsions developed in this study were stabilized by stoichiometric hydroxyapatite (HA) particles firstly prepared by a double decomposition technique in aqueous media and fully characterized. Miglyol 812, a biocompatible medium-chain triglyceride (MCT), was used as the internal phase and induced porosity after being removed by simple hydro-alcoholic washing treatment at the end of the process. The influence of several parameters (mass of HA particles, oil/water weight ratio, electrolytes concentration in the aqueous phase) on the emulsion size and stability was investigated. The aim was to define the optimized formulation conditions leading to: *i)* a kinetically stable enough emulsion that is to say without evolution during hardening, *ii)* a monodisperse (that is to say with a narrow drop size distribution) emulsion with a minimum diameter of 200 μm and *iii)* drops close enough (meaning high oil volume fractions) to induce an interconnected porosity favoring thereby osteoconductivity and bone generation [4,20]. The continuous phase of the optimized emulsions was then mineralized and two types of porous monoliths were produced and characterized: calcium phosphate monoliths (CaP) from an apatitic gel, and silica monoliths with pores covered by hydroxyapatite (Si-HA) *via* a sol-gel process for comparison (Fig. 1). Several low temperature methods of synthesis of porous polymer-CaP composites scaffolds [21,22] have been proposed in the literature, including process based on Pickering emulsions as template to perform biodegradable polymeric scaffolds [23] or hybrid microspheres [12,24]; HA-stabilized emulsions have been used to produce porous materials after sintering [11]. However, the making process proposed for the first time in the present study based on biocompatible Pickering emulsions allows the formation of porous CaP bioceramics without organic part and sintering to preserve their biocompatibility and bioactivity, and favor bone formation.

2. Materials and methods

2.1. Hydroxyapatite (HA) particles synthesis and characterization

2.2. HA synthesis

Stoichiometric hydroxyapatite (HA, $C_{10}(PO_4)_6(OH)_2$) was synthesized by double decomposition technique [25] at 90 °C and pH close to 8.5. Under continuous stirring, a phosphate salt aqueous solution (264 g of $(NH_4)_2HPO_4$, 1.3 L of deionized water) was dropwise added, during 3 h, into a calcium salt aqueous solution (787 g of $Ca(NO_3)_2$-4 H_2O, 3.3 L of deionized water). The pH was kept close to 8.5 during all the reaction by slow addition of 1.5 L of ammonia (20% wt.). The mixture was then stirred for 1 h for maturation at room temperature, washed with decarbonated water by Buchner filtration, and freeze-dried. The obtained powder was sieved (< 125 μm) and stored in a freezer (−18 °C).

2.3. HA characterization

The powders were characterized over the 400–4000 cm^{-1} range by transmittance Fourier transformed infrared (FTIR) spectroscopy (Nicolet 5700 spectrometer, ThermoElectron) with KBr pellets (2 mg sample/300 mg KBr).

X-ray diffraction (XRD) analysis was realized using a CPS 120 INEL diffractometer with the $K_{\alpha 1}$ radiation of a cobalt anticathode (λ_{Co} = 1.78892 Å). Apparent crystallite sizes were calculated from the (002) and (310) lines using the Scherrer's equation [26].

Scanning electron micrographs (SEM) of HA powders were obtained using a Philips XL30 ESEM-FEG. The particles were dispersed in ethanol and left to dry in air on a carbon grid and observed with a HITACHI-H600 (75 kV) transmission electron microscope (TEM).

The hydrodynamic diameter (D_h) and the zeta potential (ζ-potential) of HA powder in deionized water (0.7 wt%) were measured as a function of NaCl concentration (from 0 to 0.5 M) using a Zetasizer Nano ZS (Malvern Instrument).

2.4. Pickering emulsion stabilized by HA particles

2.5. Emulsification process

The synthesized HA was manually dispersed into an aqueous solution. Then Miglyol 812 (INRESA), a pharmaceutical grade MCT oil (Medium Chain Triglycerides), was added to the aqueous phase. The suspension was firstly manually mixed and then homogenized with a high-performance dispersing system (Ultra-Turrax IKA T18 homogenizer, S18–19 G rotor, 13000 rpm) at room temperature for 5 min

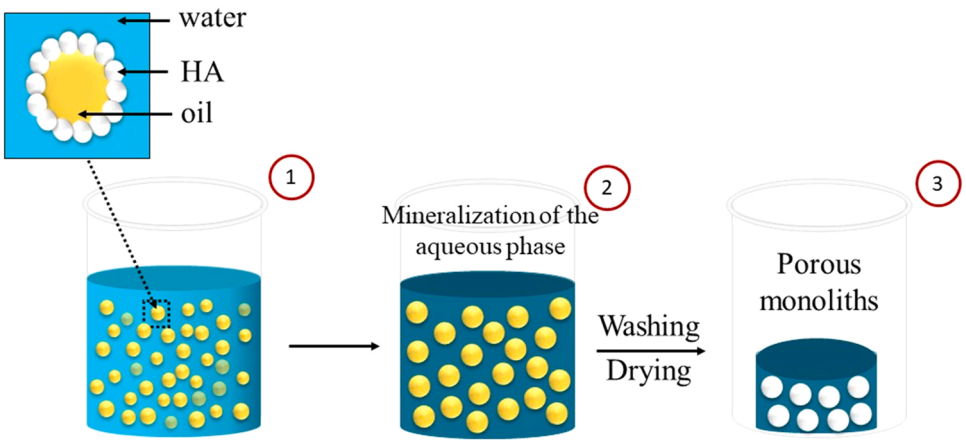

Fig. 1. Schematic representation of the process used *i.e.* biocompatible high internal phase Pickering emulsions as template to produce two types of porous monoliths: (1) Preparation of biocompatible aqueous phase/HA/oil Pickering emulsions by emulsification process at room temperature and coalescence; (2) mineralization of the continuous phase; (3) washing and drying to obtain calcium phosphate (CaP) monoliths from an apatitic gel and silica/HA (Si-HA) monoliths *via* a sol-gel process.

Several HA-stabilized Pickering emulsions were prepared by varying the mass fraction of HA particles/Miglyol 812 (1–40 $mg_{HA}/mg_{Miglyol}$), the oil/water (o/w) weight ratio (30/70, 40/60, 50/50, 60/40, 70/30, 75/25 and 80/20) and the electrolyte concentration in the aqueous phase (0–1 M NaCl). All the obtained emulsions were of the direct type *i.e.* oil-in-water emulsions. They were characterized in terms of oil droplet size distribution and kinetic stability. They were stored at ambient temperature.

2.6. Characterization of pickering emulsions stabilized by HA particles

2.6.1. Optical images. HA-stabilized emulsions were observed using a Keyence optical microscope (KEYENCE VHX-1000E) equipped with a digital camera. An emulsion sample was placed on a microscope slide. Droplets mean diameter were measured on a hundred drops, taken from about ten optical microscopy images, and the corresponding Sauter mean diameter ($D_{3,2}$) was calculated:

$$D_{3,2} = \frac{\sum_{i=1}^{i=N} d_i^3}{\sum_{i=1}^{i=N} d_i^2} \quad (1)$$

with d_i the diameter of droplet i and N the total number of drops.

2.6.2. Emulsion stability assessment. The kinetic stability of the emulsions was analyzed by static multiple light scattering (SMLS) using an optical analyzer (Turbiscan Lab Expert, Formulation, Toulouse, France). A monochromatic infrared light source ($\lambda = 880$ nm) is propagating in a cylindrical glass cell containing the sample. Two synchronous detectors collect the light scattered to detect simultaneously the transmission (T) and backscattering (BS) light flux, retransmitted in relative percentages to standards, *versus* the sample height and aging time. The BS and T signals are acquired repeatedly over time t at the whole sample height h (scanning from 0 to h with a step of Δh, h being the whole sample height). The resulting T and BS signals are time and spatial dependent. All the measurements were realized at 25 ± 0.5 °C during 10 min (1 scan per 25 s). Thirty minutes after emulsification, 20 mL of each emulsion was introduced into a 30 mL cell, without dilution and without stirring and scanned to quantify the initial emulsion stability. This first scan corresponds to D0; a second scan was performed after 70 days at ambient temperature in darkness (D70).

A specific parameter given by the apparatus provider, Turbiscan Stability Index (TSI), was used to compare and characterize the macroscopic stability of various formulations. The TSI value is calculated by summing up the evolution of T or BS (which can be due to destabilization phenomena as sedimentation, coalescence, creaming…) according to the time and height measurement at every position measured: time (hour or min) t_i, height (mm) of the emulsion h_i, following Eq. (2):

$$TSI = \frac{1}{N_h} \sum_{t_i=t_{min}}^{t_{max}} \sum_{h_i=h_{min}}^{h_{max}} |BST(t_i, \quad h_i) - BST(t_{i-1}, \quad h_i)| \quad (2)$$

with t_{max} the measurement point corresponding to the time t at which the TSI is calculated; h_{min} and h_{max} the lower and upper selected height limits of the emulsion, respectively; $N_h = \frac{(h_{max} - h_{min})}{\Delta h}$ the number of height positions in the selected zone of the scan and BST the considered signal (BS if T < 0.2%, T beyond). The TSI is equal to zero for t = 0; the higher the TSI, the less stable the emulsion.

2.7. Porous monoliths

2.8. Silica-HA (Si-HA) monoliths synthesis

Silica-HA monoliths were prepared by a sol-gel process *via* mineralization of the continuous phase of Pickering emulsions (Fig. 1). Tetraethylorthosilicate (TEOS, Sigma-Aldrich) was hydrolysed with HCl solution at a pH close to 7 with a volume ratio of 1:1 for 4 h under stirring in order to generate silicic acid $Si(OH)_4$. HA particles are stable between 6 < pH < 9 [27], thus hydrochloric acid solution (HCl 37%, Prolabo) was used (10^{-3} M) to obtain a pH equal to 7 in the aqueous phase. The emulsion was then formulated as follow: aqueous phase (0.5 M NaCl) and HA particles (10 $mg_{HA}/g_{Miglyol}$) were added to the hydrolysed TEOS with a volume ratio of 1:2. The oil phase (Miglyol 812) was added prior to emulsification to obtain an o/w weight ratio equal to 75/25. Emulsification was realized with an Ultra-Turrax stirrer at 13000 rpm for 5 min and emulsions were left at rest for 72 h to complete the sol-gel process. The resulting materials were monoliths (one self-standing piece), they were then washed with ethanol in a Soxhlet equipment before being slowly dried by air for 15 days in a desiccator at room temperature.

2.9. Calcium phosphate (CaP) monoliths synthesis

CaP monoliths were prepared from an apatitic gel *via* mineralization of the continuous phase of Pickering emulsions (Fig. 1). The synthesis of calcium phosphate (CaP) gel was based on the double decomposition method [28] by mixing two solutions previously prepared: a calcium solution (43.6 g $CaCl_2$, 2 H_2O and 0.76 g $Mg(NO_3)_2$, 6 H_2O in 250 mL)

with a phosphate and carbonate solution (109 g Na_2HPO_4 12 H_2O and 40 g $NaHCO_3$ in 750 mL). The excess of phosphate and carbonate ions acts as a pH buffer (around 7.4 in the final mixing); carbonate and magnesium ions inhibit crystals growth to preserve high surface reactivity. Once these solutions mixed, the precipitate was left to rest for maturation during 3 days at ambient temperature to allow carbonated apatite formation. The suspensions were then filtered on Buchner and washed 3 times with deionized water (1.5 L). As previously published [29], the shrinkage during drying was significant and sometimes cracks appeared. This drawback could be partly avoided by suspending the gel in a magnesium sulfate aqueous solution ($MgSO_4$, 7 H_2O; 0.5 wt% of gel in 1 L water) during few hours to control the drying rate, then filtering on Buchner and washing with deionized water (250 mL).

The Pickering emulsion was prepared according to the method previously described (*see section 1.2.1*). After 30 min, the gel was slowly incorporated to the emulsions to give a final emulsion/CaP gel weight ratio of 8, and then the mixture was stirred using Ultra-Turrax stirrer at 13000 rpm for 5 min and transferred in a polytetrafluoroethylene mold (PTFE, 26 mm in diameter × 55 mm in height). The obtained materials were monoliths (one self-standing piece), they were then slowly dried during 7 days at 40 °C to minimize shrinkage and cracks which weaken the ceramics' mechanical properties. The Mg ions adsorbed on the surface of the gel controlled the dehydration rate as previously published for dense CaP ceramics [29].

2.10. Characterization of the monoliths

The monoliths were characterized by FTIR spectroscopy, X-Ray diffraction, SEM observations previously described (*see section 1.1.2*) and by X-ray microtomography (micro-CT) with a Phoenix/GE Nanotom 180 instrument (GE Sensing, Germany), using the following parameters: 100 kV, 100 μA, 0.36° angular step. The virtual records have been reconstructed to a voxel size of 22–25 μm. A region of interest (ROI) was drawn within the reconstructed volume and analyzed with VgStudio max 2.1 and Imorph software [30]. A threshold was applied to differentiate the material and the air inside the pores. Different morphometric analyses of the ROI were realized to obtain the total porosity and the pore size distribution.

3. Results

3.1. Hydroxyapatite (HA) particles synthesis and characterization

HA particles was synthetized by double decomposition technique (see "*1. Materials and Methods*") and fully characterized in view to stabilize Pickering emulsions. HA powder was analyzed by X-Ray diffraction (Fig. 2A). The XRD pattern of the HA sample corresponds to a low crystallized apatitic phase, with no additional crystalline phase (JCPDS 9–432). Moreover, no additional phases (neither CaO nor β-TCP) were detected on the powder sintered at 1000 °C during few hours (*see* Fig. SI1 *in Supplementary Information)*; the absence of $Ca(OH)_2$ was confirmed by phenolphthalein test. The mean crystallite dimensions calculated from Scherrer's formula applied to apatitic diffraction lines (002) and (310) were evaluated: 268 ± 3 Å and 103 ± 3 Å for L(002) and L(310) lines, respectively. These values confirm that apatitic crystals were elongated along the c axis of the hexagonal structure of the apatite.

FTIR spectrum of HA powder shows characteristic bands of an apatitic calcium phosphate compound (Fig. 2B): separated split PO_4^{3-} vibration bands at 550–600 cm^{-1} (v_4), 960 cm^{-1} (v_1) and 1000–1100 cm^{-1} (v_3) and OH^- vibration at 630 and 3560 cm^{-1}, characteristic of an apatitic structure. HA spectrum also presents bands around 1450 cm^{-1} due to CO_3 vibrations characteristic of type B carbonate species resulting from the synthesis process.

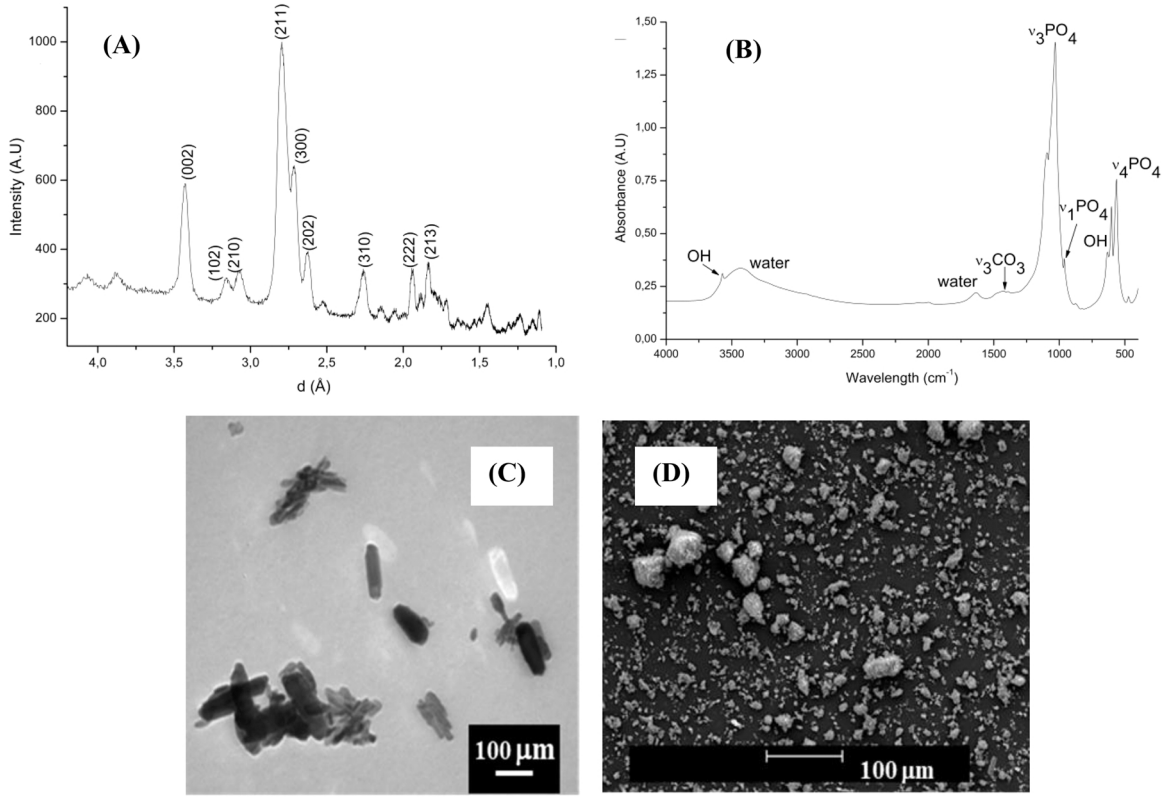

Fig. 2. (A) XRD diagram, (B) FTIR spectrum, (C) TEM and (D) SEM observations of HA powder synthesized. (hkl) indexation corresponds to pure HA phase (JCPDS 9–432).

3.2. Pickering emulsion formulation and characterization

Biocompatible Miglyol 812-in-water Pickering emulsions stabilized by previously synthesized HA particles were formulated and characterized in order to be used as template for porous monoliths. The influence of several parameters (electrolytes concentration in the aqueous phase, oil/water weight ratio and HA particles content) on emulsion drop size and stability was investigated to define the optimized formulation conditions leading to a kinetically stable enough monodisperse emulsion with a minimum diameter of 200 μm and drops close enough to lead to open porosity.

3.3. Influence of NaCl concentration in the aqueous phase

Mean droplets Sauter diameters ($D_{3,2}$) evolution was calculated from optical images of the emulsion droplets as a function of NaCl concentration (from 0 to 1 M) in the aqueous phase of emulsions (Fig. 3). HA content and o/w weight ratio were fixed at 20 $mg_{HA}/g_{Miglyol}$ and 70/30, respectively. Without NaCl, a $D_{3,2}$ of 25 ± 7 μm was obtained, while higher drop diameters (around 200 μm) were observed as soon as electrolytes were added in the aqueous phase (for example 183 ± 29 μm and 209 ± 31 μm for 0.25 M and 0.5 M, respectively).

The emulsion samples were analyzed with the optical scanning equipment Turbiscan™. The Turbiscan Stability Index (TSI) was automatically computed from the software only in the central part of the sample (emulsified phase). Table 1 shows TSI values of the emulsions as a function of NaCl concentration in the aqueous phase at D0 (30 min after emulsification) and D70 (after 70 days at ambient temperature in darkness).

Table 1
Turbiscan stability index values for HA-stabilized emulsions (20 $mg_{HA}/g_{Miglyol}$, 70/30 o/w weight ratio) with different NaCl concentrations in the aqueous phase at D0 and D70 (10 min of analysis).

NaCl in the aqueous phase (M)	TSI at D0 (30 min)	TSI at D70 (70 days)
0	1.33	35.00
0.25	0.23	4.60
0.50	0.14	1.40
0.75	0.17	2.60
1.0	0.07	2.20

Without NaCl, TSI increased quickly during the 10 min of analysis at D0 to reach the value of 1.33 at 30 min after emulsification. This stability index kept on increasing up to D70 (35), revealing that the emulsion was unstable without electrolyte. When NaCl concentration increased from 0.25 to 1.0 M, all TSI measured values were lower at D0 (≤ 0.23) than after 70 days. Nevertheless, all values remained still low (≤ 4.6), the presence of electrolyte in the aqueous phase promoted more stable HA emulsions. This behavior can be attributed to the physical organization of HA particles in agglomerates in the presence of NaCl in the aqueous phase through as salt screening effect. As an increase of particle size was observed with NaCl content until a plateau from 10^{-3} M to 1 M NaCl corresponding to HA particle aggregate size around 4.5 μm from the primary particles with a diameter of about 135 ± 40 nm (*see* Table SI1 *in Supplementary Information*). As the lowest value of TSI was observed at D70 for 0.5 M NaCl (Table 1), this concentration was

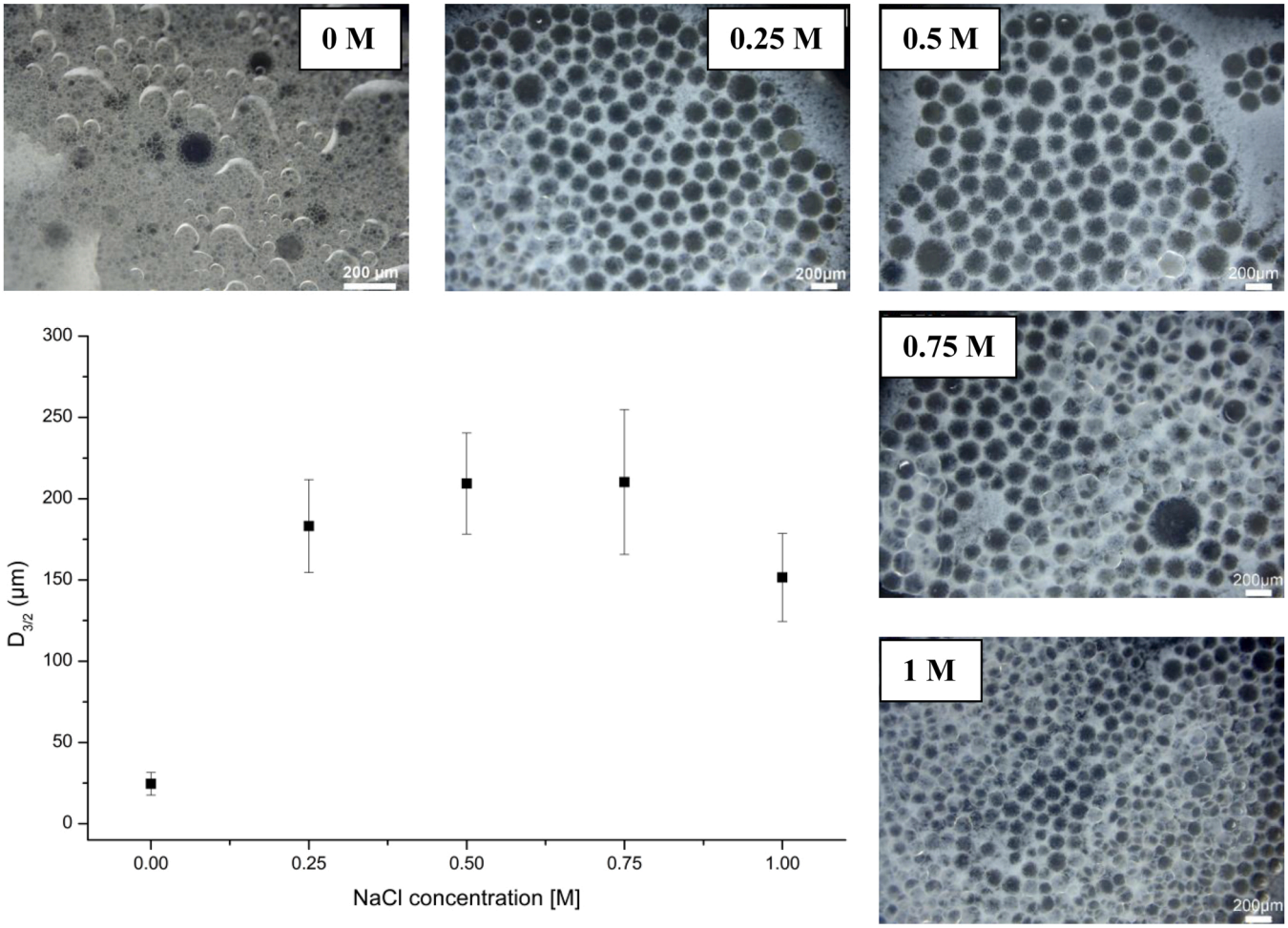

Fig. 3. Optical images and mean droplets Sauter diameter ($D_{3,2}$) of emulsion droplets as a function of NaCl concentration in the aqueous phase of the emulsions. The error bars represent the standard deviation.

selected for the following studies.

3.4. Influence of o/w weight ratio

Different HA stabilized Pickering emulsions were synthesized with 10 $mg_{HA}/g_{Miglyol}$, 0.5 M NaCl in the aqueous phase, and different o/w weight ratios: 30/70, 40/60, 50/50, 60/40, 70/30, 75/25 and 80/20. Fig. 4 shows photographs of the emulsions after emulsification (D0). At low oil content (from 30/70–60/40), due to buoyancy owing to the large droplets size and density mismatch between oil and water, the emulsions have creamed, and an excess of water can be observed at the bottom. Above the random close packing, equal to 0.64 for monodisperse emulsion and 0.71 for polydisperse emulsions, all drops are in contact and creaming is hindered (Fig. 4A). No apparent evolution was observed after 70 days (Fig. 4B).

The samples were analyzed with the optical scanning equipment Turbiscan™. The transmittance (T) and backscattering (BS) signals (%) were collected over height at D0 and D70. Turbiscan profiles and analyses' raw data are described in Fig. SI2-A and -B in *Supplementary Information*. HA-stabilized emulsion with an o/w weight ratio equal to 30/70 was not stable over time as T% increased from D0 to D70 (see Fig. SI1-*A*); the emulsion portion on the top of the sample (T% equal to zero) diminished with time because of creaming and, at the bottom, HA particles sedimentation increased (BS% increases). From the o/w weight ratio from 40/60–60/40, the aqueous part of the sample diminished as oil content increased; from 70/30–80/20, these emulsions remained stable from D0 to D70 (*see* Fig. SI1-*B in Supplementary Information*).

The TSI of each emulsion was calculated only on the remaining emulsified part (central portion *i.e.* around 30–60% of total sample height), (Table 2). The highest TSI values were observed with the lowest oil contents *i.e.* o/w weight ratio from 30/70 (0.54) to 40/60 (0.92) during the first 30 min after emulsification: these values increased up to D70 at fairly high values (5.2 and 12.0 for o/w=40/60 and 30/70, respectively), which confirms that these emulsions are not stable against creaming through time. With higher oil contents (o/w ratio from 50/50–80/20), the TSI values appeared lower beyond 30 min after emulsification (between 0.07 and 0.16), and remained low at D70 (between 0.98 and 1.5), so these samples exhibited more stable emulsified phases. High Internal Phase Emulsions (HIPE) are usually defined by a minimal internal phase ratio (ϕ) of 0.74 [31] corresponding to the highest compacity in three dimensions *i.e.* hexagonal packing of hard spheres. As drops are deformable, even higher ϕ values can be reached in emulsions. Higher ϕ values induce droplets deformation meaning the formation of flat films between drops. These films can break during drying process, thus promoting interconnection between pores [13, 31–34]. Furthermore, we notice that the oil volume fraction inside the homogeneous emulsified zone, deduced from (T) signal, is constant and equal to 76 ± 0.7%, for all emulsions from o/w ratio comprised between 30/70–60/40. This result means that the arrangement of droplets, whatever the o/w ratio chosen, is closer to compact structure rather than random close packing in the emulsified region. In order to obtain both a homogeneous emulsion in the whole volume and spherical shape of the drops, a weight content of 75% of oil (volume fraction of 76%), appear to be the optimized value and was selected for further characterization and biomaterial elaboration.

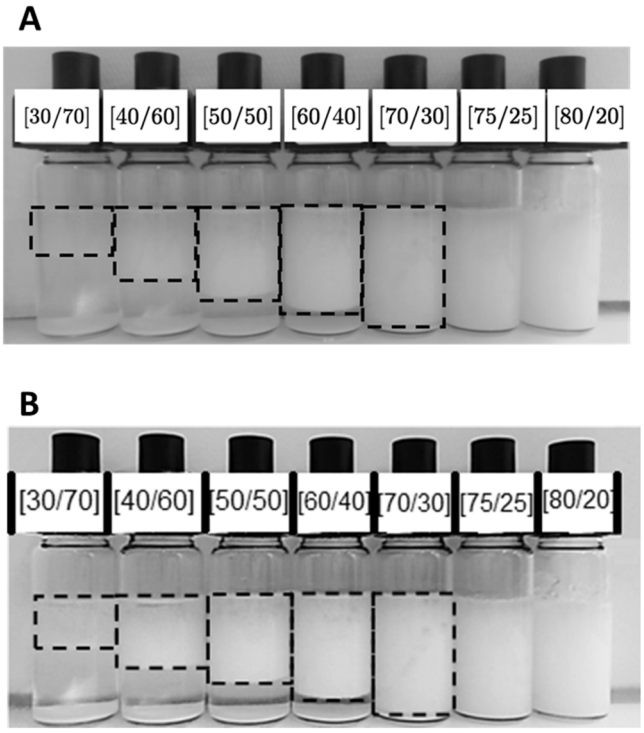

Fig. 4. Photographs of HA stabilized emulsions (10 $mg_{HA}/g_{Miglyol}$, 0.5 M NaCl) with o/w weight ratios from 30/70–80/20 at (A) D0 and (B) D70. In the hatched black rectangles are presented the emulsified areas.

Table 2
Turbiscan stability index values comparing HA-stabilized emulsions (10 $mg_{HA}/g_{Miglyol}$, 0.5 M NaCl) with o/w weight ratios from 30/70–80/20 at D0 and D70 (10 min of analysis).

o/w weight ratio	TSI at DO (30 min)	TSI at D70 (70 days)
[30/70]	0.54	12.00
[40/60]	0.92	5.20
[50/50]	0.09	1.20
[60/40]	0.16	1.00
[70/30]	0.09	1.30
[75/25]	0.07	0.98
[80/20]	0.08	1.50

3.5. Influence of HA particles content

The influence of the amount of HA added to stabilize the emulsions, with fixed o/w weight ratio (75/25) and 0.5 M NaCl in the aqueous phase, was studied from 1 to 40 $mg_{HA}/g_{Miglyol}$. Spherical droplets are observed by optical microscopy (Fig. 5) which size and homogeneity depends on HA amount.

Mean emulsion droplet diameters were measured and the variation of the mean Sauter diameter ($D_{3,2}$) was plotted as a function of HA content ($mg_{HA}/g_{Miglyol}$), (Fig. 6A). From 1–10 $mg_{HA}/g_{Miglyol}$, droplets size decreased while HA content increased. From about 10 $mg_{HA}/g_{Miglyol}$, the droplets size reached a plateau around 200 μm. Moreover, when HA content increased, standard deviation decreased (≈30 μm). The fewer the particles, the greater the standard deviation (700±270 μm for 1 $mg_{HAp}/g_{Miglyol}$), *i.e.* the larger the drop size distribution.

The samples were analyzed with the optical scanning equipment Turbiscan™. The TSI values are presented in Table 3 as a function of HA content (from 1 to 30 $mg_{HA}/g_{Miglyol}$). TSI formula was applied only in the middle region (height from ≈ 13 mm to ≈27 mm) *i.e.* in the emulsified part of each sample. At D0, the obtained TSI values were low (less than 0.3). After 70 days (D70), the emulsions stabilized with low HA contents exhibited the highest TSI values (41.0 and 9.6 for 1 $mg_{HAp}/g_{Miglyol}$ and 2 $mg_{HAp}/g_{Miglyol}$, respectively) and thus the lowest stability.

These laser-scanning turbidimetry results show that the emulsions synthesized with low HA content (1–2 $mg_{HA}/g_{Miglyol}$), and thus higher droplet sizes (D≈1000 μm and 800 μm respectively), appear unstable. The greater the HA quantity introduced into the emulsion (up to 10 $mg_{HA}/g_{Miglyol}$), the more stable the emulsion was.

By plotting the inverse of the Sauter diameter ($1/D \times 10^3$ in μm^{-1}) given in Fig. 6B as a function of the particle concentration, it is possible to delimit more precisely the domain of limited coalescence, which extends in the case of HA particles between zero and 10 $mg_{HA}/g_{Miglyol}$ (area delimited by the point of intersection between the two lines obtained from the experimental points). In the limited coalescence

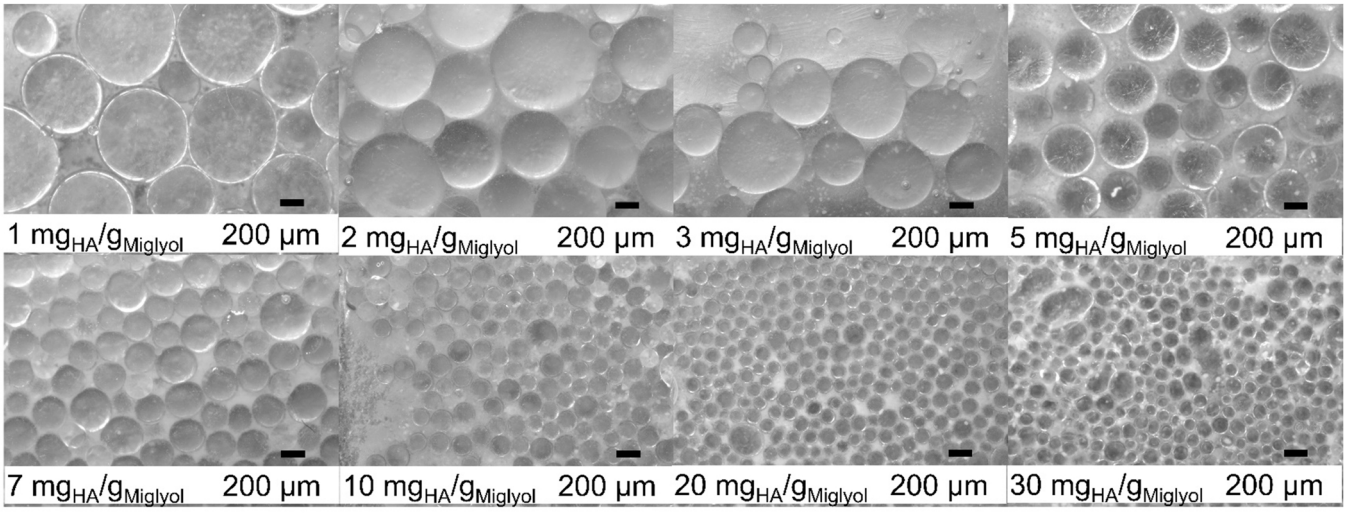

Fig. 5. Optical microscopy of emulsions (o/w weight ratio =75/25 and 0.5 M NaCl) containing various amounts of particles.

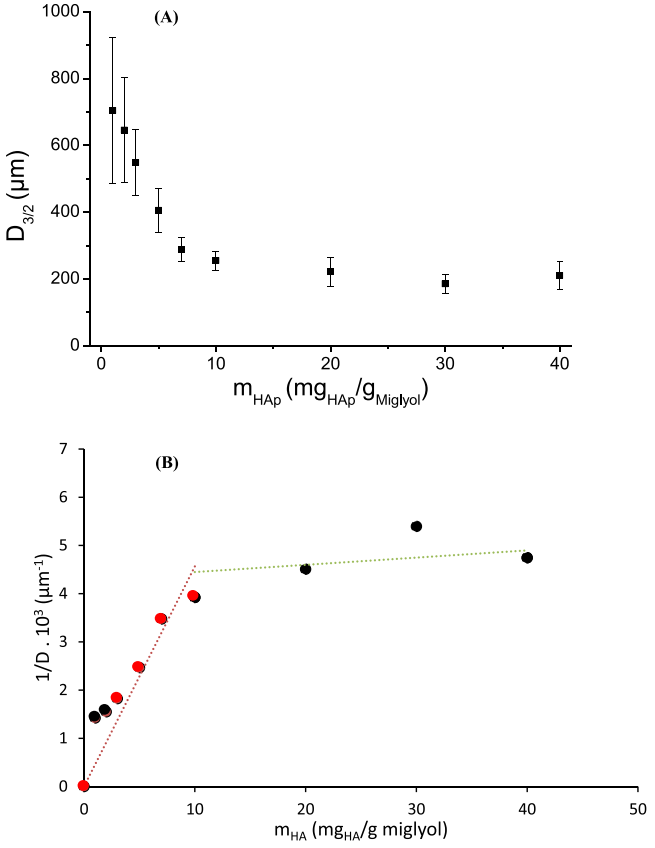

Fig. 6. A) Evolution of the mean Sauter diameter ($D_{3/2}$) of the oil droplets as a function of HA content from 1 to 40 $mg_{HAp}/g_{Miglyol}$ (o/w=75/25–0.5 M NaCl). The error bars represent the standard deviation; B) Evolution of the reverse $D_{3/2}$ of the oil droplets in function of HA content from 1 to 40 $mg_{HAp}/g_{Miglyol}$ (o/w=75/25–0.5 M NaCl). The red points (linear zone of the limited coalescence) are selected to calculate the slope. (For interpretation of the references to colour in this figure legend, the reader is referred to the web version of this article.)

domain, as previously demonstrated in the literature [35], droplets size increases until their interfaces are totally recovered by enough particles to be stable against further coalescence. In this domain, the particles mass has been found to be inversely proportional to the mean diameter of Pickering emulsion droplets [36] as represented by the linear

Table 3
Turbiscan stability index values comparing HA-stabilized emulsions (o/w=70/30, 0.5 M NaCl) with HA/Miglyiol mass ratios from 1 to 30 $mg_{HA}/g_{Miglyol}$ at D0 and D70 (10 min of analysis).

HA/ Miglyol ($mg_{HA}/g_{Miglyol}$)	TSI at DO (30 min)	TSI at D70 (70 days)
1	0.29	41.0
2	0.21	9.6
3	0.17	3.8
5	0.16	2.8
7	0.11	2.4
10	0.04	2.4
20	0.19	1.8
30	0.10	2.0

equation Eq. (3):

$$\frac{1}{D} = \frac{m_{HA} \times s_f}{6 \quad \times V_{oil}} \tag{3}$$

with m_{HA} the particles weight (g); D the droplets mean Sauter diameter (µm); s_f the droplets specific surface (meaning the droplets area that can be stabilized by 1 g of particles) and V_{oil} the dispersed phase volume (cm^3). Assuming that HA particles or agglomerates as spherical at the oil−water interface, the final drop diameter D is given by Eq. (4) [16,35,37,38]:

$$\frac{1}{D} = \frac{m_{HA}}{4 \quad \times C \times \rho_p \times d_p \times V_{oil}} = \frac{\rho_{oil}}{4 \times \rho_{HA} \times C \times d_p} \times w_{HA/oil} \tag{4}$$

with d_p the HA particules or agglomerates diameter (µm); ρ_p the density of HA particles; ρ_{oil} the density of dispersed phase; $w_{HA}/_{oil}$ the weight HA/oil ratio ($mg_{HA}/g_{Miglyol}$) and C the covered area *i.e.* the fraction of the droplet interfacial area covered by the particles [38].

Eq. (4) was proposed in the case where the solid particles adsorbed as a dense nanometric monolayer of close packed silica spheres or in the case of silica aggregates stabilized emulsions [35,39]. As described [15,35] in this domain, solid particles or aggregates are fully adsorbed at the drops surface of Pickering emulsions, no residual solid particle is observed in the aqueous phase, the resulting emulsions are stable against further coalescence with no drop size evolution with time, this regime named limited coalescence domain extends up to 10 $mg_{HA}/g_{Miglyol}$. Beyond this amount, there are enough particles to directly stabilize the drop size distribution generated by the stirring device.

As previously noticed, in the context of biomaterials elaboration with

a view for bone reconstruction [4], droplets size of at least about 200 µm will be required to promote the proliferation of bone cells. A concentration of 10 $mg_{HAp}/g_{Miglyol}$ was then chosen in the rest of this study to remain in the limited coalescence domain, avoiding excess of non-adsorbed particles, while targeting drop sizes of around 200 µm. Thus, the HA-stabilized emulsions used in this work to develop porous monoliths were formulated using 10 $mg_{HA}/g_{Miglyol}$, o/w ratio equal to 75/25 and 0.5 M NaCl in the aqueous phase; this formulation led to a monodisperse and stable over time emulsion with an average droplet size of 255 ± 28 µm in diameter.

3.6. Porous monoliths preparation and characterization

The continuous phase of the optimized emulsions was then mineralized and two types of porous monoliths were produced and characterized: calcium phosphate monoliths (CaP) from an apatitic gel, and silica-HA monoliths (Si-HA) *via* a sol-gel process for comparison (Fig. 1).

3.7. Si-HA monoliths

XRD diagrams of the Si-HA monoliths *(see* Fig. SI2 *in Supplementary Information)* showed a broad peak, characteristic of silica amorphous compound, between 3 and 5 Å, with additional fine crystalline apatite peaks, demonstrating the presence of the HA used to stabilize the precursor emulsions of the synthesized monoliths.

SEM observations of the monoliths (Fig. 7A) show a porous and totally interconnected structure. The spherical pores measured by CT present mean diameters between 1 mm and a hundred µm with high polydispersity. Few pores could be induced by air bubbles trapped during emulsification by Ultra-Turrax® stirrer at 13000 rpm and the fast gelation process difficult to control. The conjunction between air bubbles trapping and non-constant shear stress applied to the droplet due to simultaneous gelling may explain the observed pore sizes polydispersity.

SEM observations inside the pores (Fig. 7B) show a chemical contrast suggesting that they are coated with HA particles from the starting emulsion. EDX analyses performed on the light zones, identified as HA particles, confirm the presence of calcium and phosphate as main components, meaning that pores are indeed internally covered with HA particles. For bone regeneration, this is an important feature because it allows contact between HA and cells and thus the bioactivity of monoliths. On the contrary, from EDX analysis performed in the darker parts corresponding to the inter-porosity, silica appears the only component.

Si-HA monoliths were investigated by micro-CT (Fig. 8A) which shows a porous and interconnected network in accordance with SEM observations. Using Imorph software calculation [30], an average pores size of 283 ± 131 µm was obtained, close to the droplets mean diameter of the initial emulsion used as template, with a total porosity of 75% (± 2) equal to oil content in the mixture (o/w weight ratio equal to 75/25, see Section 1). The good agreement between the emulsion and the monolith indicates that the emulsion remained stable during hardening and that no shrinkage was observed for Si-HA monoliths. However high pore size polydispersity was obtained as explained previously. This can originate from the difficulty to control pores size formation of silica network, especially during network stabilization (air trapping due to fast gelation and non-constant shear stress applied to the droplets due to the on-going gelation process that intrinsically varies the system viscosity).

3.8. CaP monoliths

XRD diagram of CaP monoliths obtained by addition of an apatitic calcium phosphate gel (Fig. 9A) shows pure apatitic compounds with no additional peak, and presents lower intensity and broader peaks suggesting a low crystallinity, characteristic of poorly crystallized biomimetic apatites. The crystallite size calculated using Scherrer's formula from (002) and (310) lines are 298 ± 3 Å and 113 ± 3 Å for the L(002) and L(310) lines, respectively.

FTIR spectra of CaP monoliths shows characteristic vibration bands of poorly crystalline apatite (Fig. 9B), [17,40,41]: PO_4^{3-} stretching modes at 469 (ν_2), 563 – 603 (ν_4), 962 (ν_1), and 1000 – 1100 cm– 1 (ν_3). The weaker band at 872 cm^{-1} can be assigned to hydrogenophosphate HPO_4^{2-} vibration, characteristic of non-stoichiometric apatite compared with stoichiometric HA spectrum (Fig. 2B). Moreover, vibration bands can be seen around 870, 1420 and 1457 cm^{-1} due to CO_3 vibrations characteristic of non-apatitic carbonates and type B

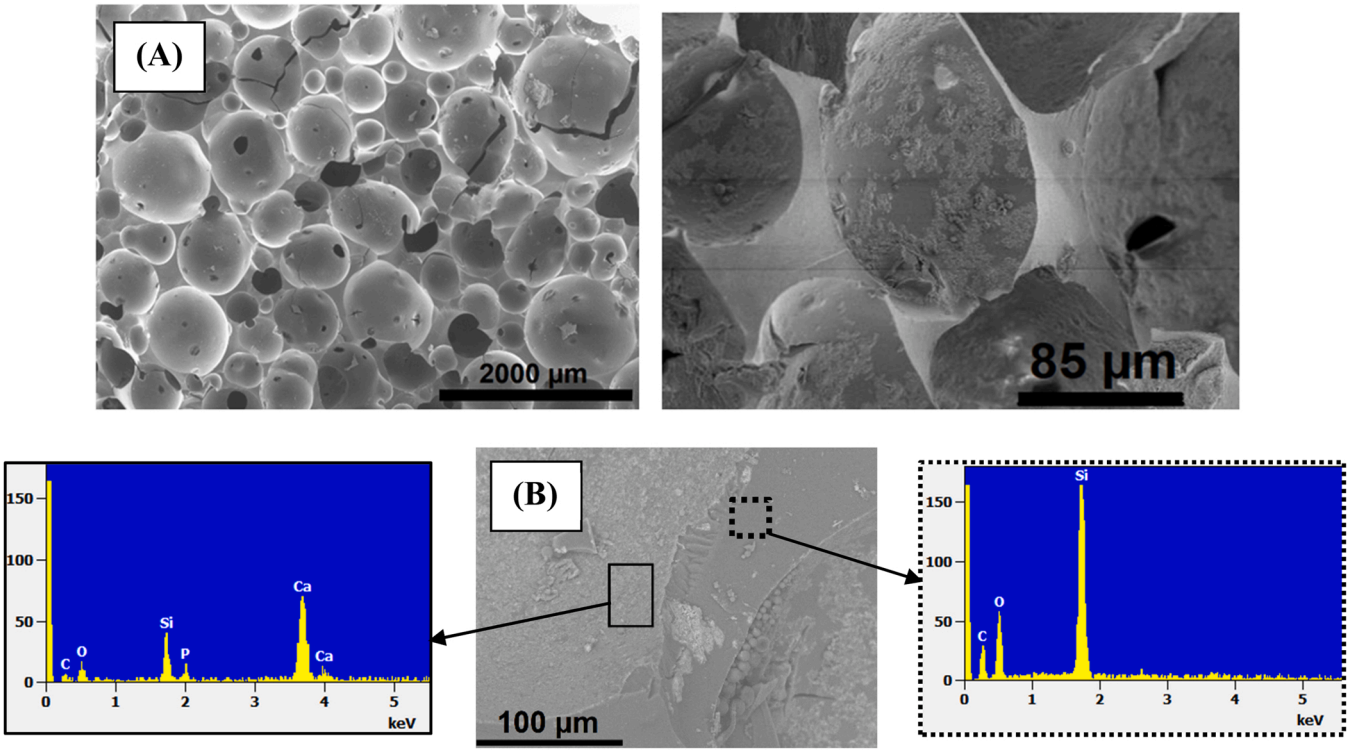

Fig. 7. (A) SEM observations and (B) SEM/EDX analysis of Si-HA monoliths.

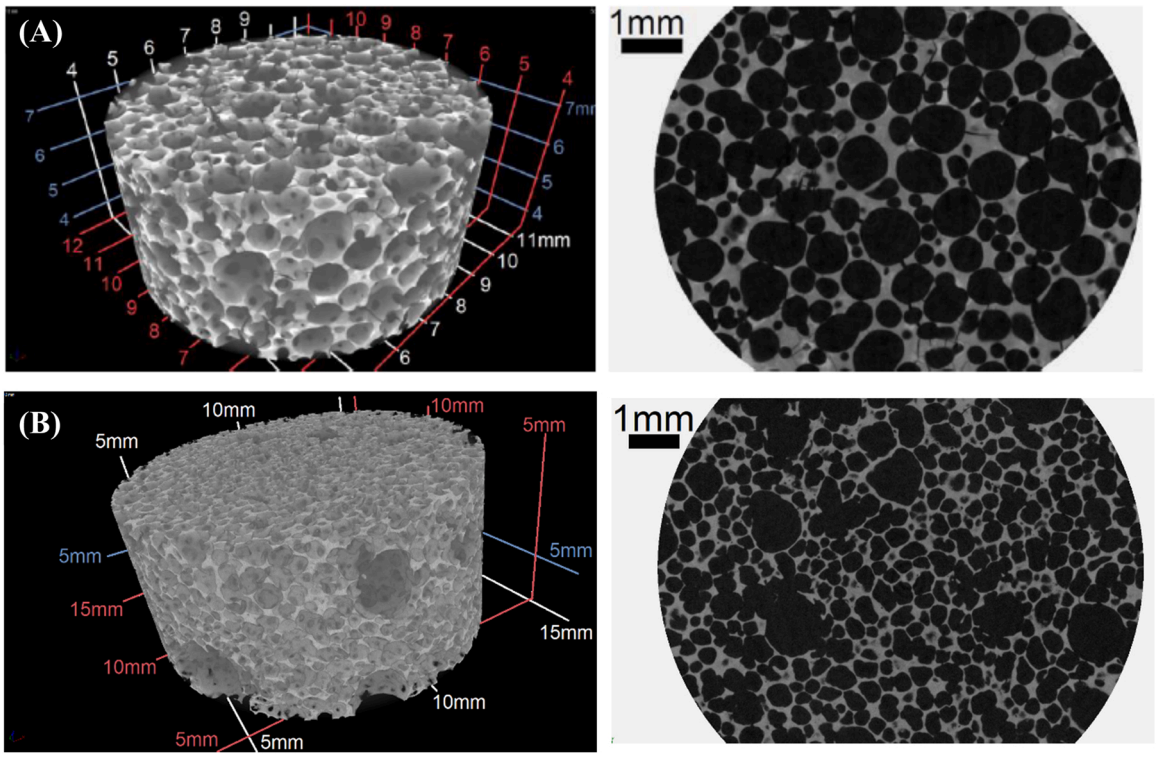

Fig. 8. Micro-CT analysis and cross-section of (A) Si-HA monoliths and (B) CaP monoliths.

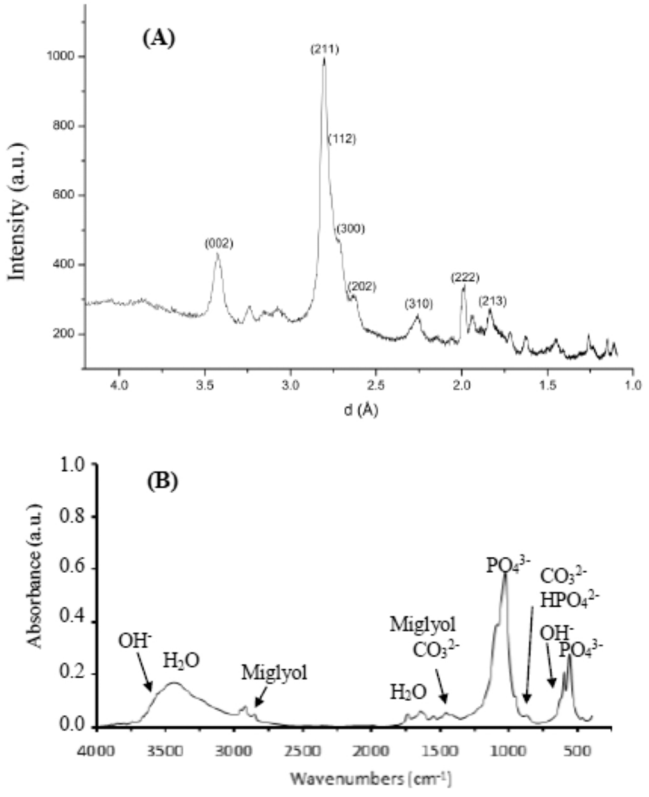

Fig. 9. (A) X-ray diffraction diagram and (B) FTIR spectrum of CaP monoliths.

carbonate species. In addition, small OH^- vibration bands are barely detected at 3567 and 630 cm^{-1} which can result from stoichiometric HA powders. In addition, a wide spread band from 3000 to 3700 cm^{-1} and a weaker one around 1700 cm^{-1} are attributed to water due to the drying process and the low crystallinity of the obtained apatitic monoliths; some organic residues bands (at 2930 cm^{-1} due to CH_2 stretching symmetric and asymmetric modes and around 1700 cm^{-1} due to the CO stretching ones) can also be attributed to Miglyol residues.

SEM observations of obtained CaP monoliths (Fig. 10A) show interconnected quite monodisperse porosity with mean size diameters of few hundred μm. Compared with HA-Si monoliths, the pores have lost their spherical shape: calcium phosphate gel contains around 90% of water and an important shrinkage is observed during drying (about 70% by mass). Moreover, mean size diameters of the pores appears more homogeneous than for HA-Si monoliths. SEM/EDX analysis (Fig. 10B) show the presence of calcium and phosphate compounds in the monoliths but does not allow differentiation between HA particles from initial emulsion and biomimetic apatite from the gel, because of their chemical similarities.

HA monolith cross section of CaP monoliths analyzed by micro-CT (Fig. 8B) revealed a homogeneous pore size distribution, as seen by SEM observation (but only for one slice due to the limitation of the SEM technique), suggesting that CaP gel-based process does not lead to the initial emulsion destabilization. However, some bigger pores can be observed which can explain the greater fragility of CaP monoliths compared to Si-HA ones or again by incorporation of air bubbles. Using Imorph software calculation [30], the average pores size of 188 ± 103 μm is obtained, lower than the initial Pickering emulsions droplets diameter. A further fragmentation of the drops resulting from additional stirring after incorporation of the gel into the emulsion could explain the lower pore sizes compared to the drop sizes that could also be due to contraction. The total porosity determined by IMorph calculation is about 66% (± 3).

4. Discussion

In this study, biocompatible Pickering emulsions stabilized by pure HA particles are used as template to obtain porous monoliths. Even if HA particles observed by TEM are rod-shaped, in suspension in water they tend to agglomerate, and electrolytes concentration favors HA

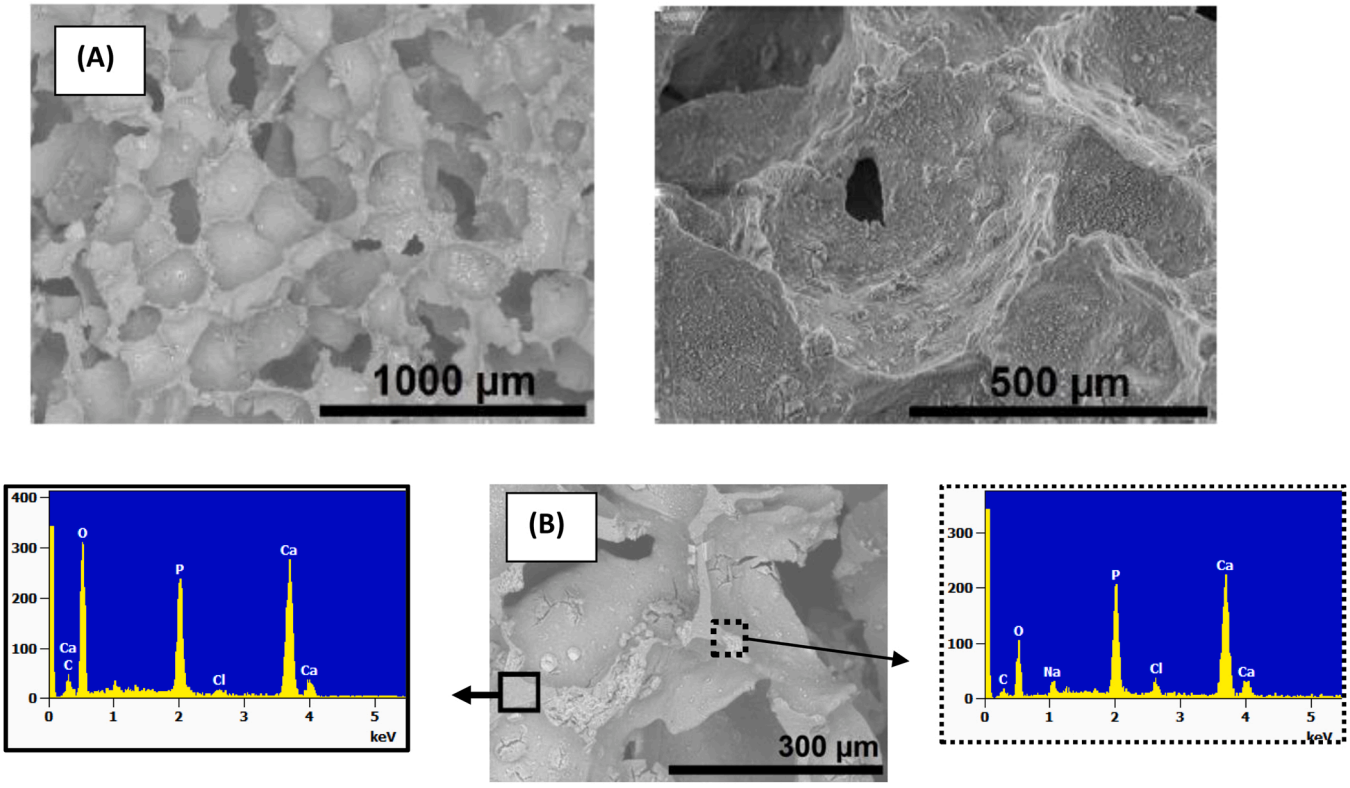

Fig. 10. (A) SEM observations and (B) SEM/EDX analysis of CaP monoliths.

aggregation. Similar observations were reported by various authors [42]. Moreover, zeta potential of HA particles increased with NaCl concentration (see Table SI1) leading to their aggregation. Tham et al. [43] stated similar results for HA particles in electrolytes solution (KNO_3) and evidenced a critical flocculation concentration (CFC). In the present study, this CFC is observed for 10^{-3} M NaCl in HA particles suspended in water; beyond 10^{-3} M NaCl aggregates size remains stable (around 4.5 µm). The DLVO theory (Derjaguin, Landau, Verwey and Overbeek) [44,45] takes into accounts the interactions between those particles in aqueous media based on two forces: electrostatic repulsions and Van der Waals attractions. Electrolyte concentration involves an increase of the zeta potential (*i.e.* decrease of the absolute value), related to the screening of electrostatic repulsions (assigned by previous authors to a compression of the double layer (Stern layer compression) [43,46]). Indeed, the Debye length decreased from 9.5 nm to 0.4 nm when the NaCl concentration increased from 10^{-3} M to 0.5 M.

The control of droplet size and stability of solid emulsions has been studied by several authors for silica [16,35], $CaCO_3$ particles [47,48] or HA [11], and particles content appears one of the main parameter. For most of solid stabilized Pickering emulsions, the increase of particles content involves a decrease of droplets diameters improving emulsion stability against creaming. The synthesized emulsions with low HA content (1 – 2 $mg_{HA}/g_{Miglyol}$) leads to high droplets sizes (D≈1000 µm and 800 µm respectively) with no particles in excess (limited coalescence domain). On the other hand, large amount of HA (>10 $mg_{HA}/g_{Miglyol}$) lead to smaller drop sizes (200 µm) with an excess of particles in the continuous phase. At the limit between the two regimes (10 $mg_{HA}/g_{Miglyol}$), the drops size is close to the target value of 200 µm with no particles in excess meaning that the amount of particles has been optimized.

In the limited coalescence domain, from the slope measured in Fig. 6B (0.44 µm $^{-1}$ in the linear zone of the limited coalescence), the calculated specific surface defined in Eq. (3) is $s_f = 2.8\ m^2/g$ HA, which means 1 g HA stabilize 2.8 m^2 of the droplet surface. The arrangement of the particles around the droplets are not known, which can be spherical agglomerates or elementary rod-shaped particles. In this paper, we focus on the hypothesis that stabilization is governed by adsorption of spherical agglomerates on droplets surface, as HA particles tend to agglomerate in water, especially when electrolyte is added. Following the spherical-shape agglomerates adsorbed at the interface hypothesis, the coverage rate C of the drops and/or the size of the particle-agglomerates covering these drops can be estimated. In the limited coalescence zone (until 10 $m_{HA}/g_{Miglyol}$, see Fig. 6B), the evolution of 1/D (the reverse of the droplets diameter) is linear as a function of $m_{HA}/g_{Miglyol}$. Thus, from Eq. (4), the slope is related to the coverage rate C and to the diameter dp of the HA agglomerates:

$$slope = \frac{\rho_{oil}}{4 \times \rho_{HA}} \times \frac{1}{C \times d_p} \quad (5)$$

Taking the values of the slope in the linear zone of the limited coalescence (Fig. 6B), the density of the HA particles measured by helium pycnometer (2.92 ± 0.01 $g.cm^{-3}$), and the density of the oil (0.95 $g.cm^{-3}$):

$$C.d_p = 0.183 \quad \mu m \quad (6)$$

Considering the droplets are stabilized by HA agglomerates in the limited coalescence zone, and the size of agglomerates estimated at about 4.5 µm in 0.5 M NaCl as seen previously, a coverage rate around 4% is obtained from Eq. (5). However, this value appears very low to allow for optimal coverage and therefore significant stability of Pickering emulsions. In the limited coalescence zone, a coverage rate less than or equal to 0.9 is generally observed as this is the maximum stacking value of single-ply spherical particles in accordance with the literature [49]. Considering a maximum coverage rate of 0.9 and the achievement of a single layer, then the average size of the supposed spherical agglomerated would be around 200 nm calculated from Eq. (6).

Agglomeration of HA particles is a key parameter of Pickering

emulsions properties, as the formation of particles agglomerates between the oil droplets are responsible of solid emulsion stability and manage coalescence phenomenon as explained by previous authors: the adsorbed layer of HA particles forms a rigid coating around liquid droplets and mechanical strength of such solid layer comes from particles aggregation [16,50]. Moreover, the droplets size and stability of Pickering emulsions are controlled by adsorption process of solid particles at the o/w interface and thus requires the partial wetting of the solid particles by water and oil, which is related to interfacial tension and size of HA particles [11,16].

Therefore, several parameters were studied to optimize HA stabilized emulsions to obtain bioceramics according to the criteria defined previously: interconnected pores having a minimum size of 200 μm to promote osteoconduction. On the one hand, using HA-stabilized Pickering emulsions and sol-gel process, porous monoliths of HA-silica with control size porosity were obtained. The mean size diameter of the pores was close to the droplets size of the initial emulsion, interconnected, with spherical shape, but with high polydispersity due to sol-gel and drying process. The pores of the bioinert silica-based monoliths are covered by bioactive HA coating. The size, interconnection and inner HA coating of the obtained porosity will favour osteo-integration of the monoliths in biological media. On the other hand, using HA-stabilized Pickering emulsions and apatitic gel process, porous low crystalline apatite bioceramics were obtained with control droplet size. This low temperature process preserves the high surface reactivity of the biomimetic apatite-like mineral part of bone. The porosity obtained was quite monodisperse and interconnected, as no destabilization of the initial emulsions was involved. The size, interconnection and biomimetic apatites would favor osteo-conduction and biororbability of the monoliths in biological media. However, the pore shape of the CaP-monoliths appeared not spherical (ellipsoidal shape); this can be explained by the effect of gravity during drying (deformation of oil droplets) in suspension in low-viscous CaP-gel, and/or by the anisotropic shrinkage observed for CaP monoliths with the drying process (70% of weight loss, 45% of height loss and 50% of diameter loss) which can be explained by the crystallization of apatite during drying. Moreover, the mean size diameter appeared lower than the size of the initial emulsion droplets, as previously observed by Destribats *et al.* [13] for silica foams and explained by the high shrinkage observed during drying and solidification. The drop/macropore diameters ratio, equal to 1.36 for the CaP monoliths using the average values, up to 3 considering the large standard deviations observed leads to a contraction factor (or microscopic shrinkage rate, estimated from the cube of the drop/macropore diameter ratio) equal to 2.5 using the average value, up to 9. This contraction factor detected at a micrometer scale can be compared with the macroscopic volume contraction, calculated from the CaP monoliths dimensions and equal to 9 ± 1. Contrarily to what was observed for silica foams [13], these microscopic and macroscopic factors are different, due to the fact that the wall are not taken into account in the calculus, and/or in the case of the CaP monoliths because of the anisotropy of the shrinkage observed.

Low temperature processes provided macroporous bioceramics with controlled composition and porosity. It can be noticed that a common drawback to all calcium phosphate porous bioceramics is their low mechanical properties that largely limit their clinical use to non-major load-bearing parts of the skeleton, even when calcium phosphate scaffolds are consolidated by sintering [2]. This was also the case for the monoliths obtained in the present study as they were fragile whatever the used mineralization process (Si-HA or CaP). Despite this fragility, they should be suitable for filling defects on bone sites where mechanical stress is low as in maxillofacial regeneration for example.

5. Conclusion

In this work, biocompatible Pickering emulsions were successfully stabilized by hydroxyapatite particles and used to obtain low temperature apatitic bioceramics with tunable porosity *via* low temperature synthesis process. The oil volume fraction, particle concentration, and ionic strength of the biocompatible emulsions were optimized through a series of drop-size distribution and emulsion stability tests. At optimal preparation conditions (10 $mg_{HA}/g_{Miglyol}$, dispersed oil fraction equal to 0.75 and 0.5 M NaCl) monodisperse and stable high internal phase Pickering emulsions with around 250 μm mean diameter droplets were generated. Using these emulsions as a template, two types of porous bioceramics material with a hierarchical pore structure was obtained by low temperature process and simple drying: calcium phosphate monoliths (CaP) from an apatitic gel, and silica/HA monoliths *via* a sol-gel process for comparison. This low temperature process provides bioceramics able to perform bioactivity and bioresorption *in-vivo*, and could feature a drug or other therapeutic ions-delivery capability for filling bone defects in maxillofacial or orthopedic surgery. In the case of mineralization using silica precursors, in the HA-stabilized emulsion, a silica porous monolith matrix coated by HA was obtained. In the case of mixing an apatitic gel with the HA-stabilized emulsion, the monolith is only made of biomimetic apatite of high reactivity. The morphology of these materials have been studied. In both cases, the self-standing materials exhibited an open porosity with accessible pore of about 200 μm in diameter. The performances of the CaP materials elaborated in this paper for bone regeneration applications will be demonstrated in future studies.

CRediT authorship contribution statement

K. Pascaud: Conceptualization, investigation, methodology, formal analysis, Vizualization, Writing. **M. Mercé**: Investigation, formal analysis. **A. Roucher:** Methodology, Supervision. **M. Destribats:** Conceptualization, Methodology. **R. Backov:** Validation, Supervision. **V. Schmitt:** Validation, Supervision. **R. Sescousse:** Conceptualization, Validation, Supervision, Writing – original/review. **F. Brouillet:** Conceptualization, Validation, Supervision, Writing – original/review. **S. Sarda:** Conceptualization, Validation, Supervision, Funding acquisition, Project administration, Vizualization, Writing – original/review. **M.I. Ré**: Conceptualization, Validation, Supervision, Funding acquisition, Project administration, Writing – original/review.

Declaration of Competing Interest

The authors declare that they have no known competing financial interests or personal relationships that could have appeared to influence the work reported in this paper.

Acknowledgements

The authors wish to thank the Fédération FERMAT (FR3089, France), as well as C Tenailleau, B. Duployer (CIRIMAT) for micro-CT experiments and S. Party (RAPSODEE/IMT Mines Albi) for DLS analysis.

Appendix A. Supporting information

Supplementary data associated with this article can be found in the online version at doi:10.1016/j.colsurfa.2022.128748.

References

[1] M. Sladkova, M. Palmer, C. Öhman, R.J. Alhaddad, A. Esmael, H. Engqvist, G.M. de Peppo, Fabrication of macroporous cement scaffolds using PEG particles: in vitro evaluation with induced pluripotent stem cell-derived mesenchymal progenitors, Mater. Sci. Eng.: C. 69 (2016) 640–652.
[2] F. Baino, G. Novajra, C. Vitale-Brovarone, Bioceramics and scaffolds: a winning combination for tissue engineering, Front. Bioeng. Biotechnol. 3 (2015) 202.
[3] E. Champion, Sintering of calcium phosphate bioceramics, Acta Biomater. 9 (4) (2013) 5855–5875.
[4] R.A. Perez, G. Mestres, Role of pore size and morphology in musculo-skeletal tissue regeneration, Mater. Sci. Eng.: C. 61 (2016) 922–939.

[5] A. Bignon, J. Chouteau, J. Chevalier, G. Fantozzi, J.-P. Carret, P. Chavassieux, G. Boivin, M. Melin, D. Hartmann, Effect of micro-and macroporosity of bone substitutes on their mechanical properties and cellular response, J. Mater. Sci.: Mater. Med. 14 (12) (2003) 1089–1097.

[6] Y. Tang, Y. Tang, C. Lv, Z. Zhou, Preparation of uniform porous hydroxyapatite biomaterials by a new method, Appl. Surf. Sci. 254 (17) (2008) 5359–5362.

[7] R. Backov, M. Mercé, V. Schmitt, S. Sarda, J. Soulié, Synthèse de matériaux poreux monolithiques biocompatibles, French Patent Application, 07642–01, 2015.

[8] W. Ramsden, Separation of solids in the surface-layers of solutions and 'suspensions'(observations on surface-membranes, bubbles, emulsions, and mechanical coagulation).—Preliminary account, Proc. R. Soc. Lond. 72 (477–486) (1904) 156–164.

[9] S.U. Pickering, Cxcvi.—emulsions, journal of the chemical society, Transactions 91 (1907) 2001–2021.

[10] Y. Yang, Z. Fang, X. Chen, W. Zhang, Y. Xie, Y. Chen, Z. Liu, W. Yuan, An overview of Pickering emulsions: solid-particle materials, classification, morphology, and applications, Front. Pharmacol. 8 (2017) 287.

[11] S. Fujii, M. Okada, T. Furuzono, Hydroxyapatite nanoparticles as stimulus-responsive particulate emulsifiers and building block for porous materials, J. Colloid Interface Sci. 315 (1) (2007) 287–296.

[12] S. Fujii, M. Okada, H. Sawa, T. Furuzono, Y. Nakamura, Hydroxyapatite nanoparticles as particulate emulsifier: fabrication of hydroxyapatite-coated biodegradable microspheres, Langmuir 25 (17) (2009) 9759–9766.

[13] M. Destribats, B. Faure, M. Birot, O. Babot, V. Schmitt, R. Backov, Tailored silica macrocellular foams: combining limited coalescence-based pickering emulsion and sol–gel process, Adv. Funct. Mater. 22 (12) (2012) 2642–2654.

[14] R. Lopetinsky, Solids-stabilized emulsions: a review, Colloïd. Part. Liq. Interfaces (2006) 186–224.

[15] J. Wu, G.H. Ma, Recent studies of Pickering emulsions: particles make the difference, Small 12 (34) (2016) 4633–4648.

[16] Y. Chevalier, M.-A. Bolzinger, Emulsions stabilized with solid nanoparticles: pickering emulsions, Colloids Surf. A: Physicochem. Eng. Asp. 439 (2013) 23–34.

[17] C. Rey, C. Combes, C. Drouet, H. Sfihi, A. Barroug, Physico-chemical properties of nanocrystalline apatites: Implications for biominerals and biomaterials, Mater. Sci. Eng.: C. 27 (2) (2007) 198–205.

[18] C. Rey, C. Combes, C. Drouet, S. Cazalbou, D. Grossin, F. Brouillet, S. Sarda, Surface properties of biomimetic nanocrystalline apatites; applications in biomaterials, Prog. Cryst. Growth Charact. Mater. 60 (6) (2014) 3e73.

[19] A. Al-Kattan, F. Errassifi, A.M. Sautereau, S. Sarda, P. Dufour, A. Barroug, I. Dos Santos, C. Combes, D. Grossin, C. Rey, C. Drouet, Medical potentialities of biomimetic apatites through adsorption, ionic substitution, and mineral/organic associations: three illustrative examples, Adv. Eng. Mater. 12 (7) (2010) B224–B233.

[20] T. Adachi, Y. Osako, M. Tanaka, M. Hojo, S.J. Hollister, Framework for optimal design of porous scaffold microstructure by computational simulation of bone regeneration, Biomaterials 27 (21) (2006) 3964–3972.

[21] M. Schardosim, J. Soulié, D. Poquillon, S. Cazalbou, B. Duployer, C. Tenailleau, C. Rey, R. Hübler, C. Combes, Freeze-casting for PLGA/carbonated apatite composite scaffolds: structure and properties, Mater. Sci. Eng.: C. 77 (2017) 731–738.

[22] B.I. Oladapo, I.A. Daniyan, O.M. Ikumapayi, O.B. Malachi, I.O. Malachi, Microanalysis of hybrid characterization of PLA/cHA polymer scaffolds for bone regeneration, Polym. Test. 83 (2020), 106341.

[23] Y. Hu, S. Zou, W. Chen, Z. Tong, C. Wang, Mineralization and drug release of hydroxyapatite/poly (l-lactic acid) nanocomposite scaffolds prepared by Pickering emulsion templating, Colloids Surf. B: Biointerfaces 122 (2014) 559–565.

[24] M. Iafisco, B. Palazzo, T. Ito, M. Otsuka, M. Senna, J.M. Delgado-Lopez, J. Gomez-Morales, A. Tampieri, M. Prat, L. Rimondini, Preparation of core–shell poly (l-lactic) acid-nanocrystalline apatite hollow microspheres for bone repairing applications, J. Mater. Sci.: Mater. Med. 23 (11) (2012) 2659–2669.

[25] J.C. Trombe, Contribution à l'étude de la décomposition et la réactivité de certaines apatites hydroxylées carbonatées ou fluorées alcalino-terreuses, UPS, Toulouse, france, 1972.

[26] P. Scherrer, Estimation of the size and internal structure of colloidal particles by means of röntgen, Nachr. Ges. Wiss. Göttingen 2 (1918) 96–100.

[27] J.C. Elliott, Structure and chemistry of the apatites and other calcium orthophosphates, Elsevier, Amsterdam ed, 1994.

[28] C. Rey, A. Hina, A. Tofighi, M.J. Glimcher, Maturation of poorly crystalline apatites: chemical and structural aspects in vivo and in vitro, Cells Mater. 5 (4) (1995) 345–356.

[29] S. Sarda, A. Tofighi, M.C. Hobatho, D. Lee, C. Rey, Associations of low temperature apatite ceramics and proteins, Phosphorus Res. Bull. 10 (1999) 208–2013.

[30] E. Brun, J. Vicente, F. Topin, R. Occelli, IMorph: a 3D morphological tool to fully analyse all kind of cellular materials, Cell. Met. Struct. Funct. Appl. (2008).

[31] N.R. Cameron, High internal phase emulsion templating as a route to well-defined porous polymers, Polymer 46 (5) (2005) 1439–1449.

[32] N. Cameron, D. Sherrington, High internal phase emulsions (HIPEs)—Structure, properties and use in polymer preparation, Biopolym. Liq. Cryst. Polym. phase Emuls. (1996) 163–214.

[33] S.D. Kimmins, N.R. Cameron, Functional porous polymers by emulsion templating: recent advances, Adv. Funct. Mater. 21 (2) (2011) 211–225.

[34] G. Ceglia, L. Mahéo, P. Viot, D. Bernard, A. Chirazi, I. Ly, O. Mondain-Monval, V. Schmitt, Formulation and mechanical properties of emulsion-based model polymer foams, Eur. Phys. J. E 35 (4) (2012) 1–11.

[35] S. Arditty, C. Whitby, B. Binks, V. Schmitt, F. Leal-Calderon, Some general features of limited coalescence in solid-stabilized emulsions, Eur. Phys. J. E 11 (3) (2003) 273–281.

[36] V. Schmitt, S. Arditty, J. Giermanska-Kahn, F. Lealcalderon, Les émulsions de Pickering, Formulation cosmétique, EDP sciences, 2020, pp. 17–30.

[37] V. Schmitt, M. Destribats, R. Backov, Colloidal particles as liquid dispersion stabilizer: pickering emulsions and materials thereof, Comptes Rendus Phys. 15 (8–9) (2014) 761–774.

[38] M. Destribats, S. Gineste, E. Laurichesse, H. Tanner, F. Leal-Calderon, V. Héroguez, V. Schmitt, Pickering emulsions: what are the main parameters determining the emulsion type and interfacial properties? Langmuir 30 (31) (2014) 9313–9326.

[39] J. Frelichowska, M.-A. Bolzinger, Y. Chevalier, Effects of solid particle content on properties of o/w Pickering emulsions, J. Colloid Interface Sci. 351 (2) (2010) 348–356.

[40] D. Eichert, C. Drouet, H. Sfihi, C. Rey, C. Combes, Nanocrystalline apatite-based biomaterials: synthesis, processing and characterization, Biomater. Res. Adv. (2007) 93–143.

[41] D. Eichert, C. Drouet, H. Sfihi, C. Rey, C. Combes, Nanocrystalline apatite-based biomaterials: synthesis, processing and characterization, Biomater. Res. Adv. 93 (2008).

[42] D. Wang, M. Paradelo, S.A. Bradford, W.J. Peijnenburg, L. Chu, D. Zhou, Facilitated transport of Cu with hydroxyapatite nanoparticles in saturated sand: effects of solution ionic strength and composition, Water Res. 45 (18) (2011) 5905–5915.

[43] C.Y. Tham, W.S. Chow, Poly (lactic acid) microparticles with controllable morphology by hydroxyapatite stabilized pickering emulsions: effect of pH, salt, and amphiphilic agents, Colloids Surf. A: Physicochem. Eng. Asp. 533 (2017) 275–285.

[44] B. Derjaguin, L. Landau, Theory of the stability of strongly charged lyophobic sols and of the adhesion of strongly charged particles in solutions of electrolytes, Prog. Surf. Sci. 43 (1–4) (1993) 30–59.

[45] E.J.W. Verwey, Theory of the stability of lyophobic colloids, J. Phys. Chem. 51 (3) (1947) 631–636.

[46] M. Elimelech, J. Gregory, X. Jia, Particle deposition and aggregation: measurement, modelling and simulation, Butterworth-Heinemann, 2013.

[47] Y. Zhu, L.-H. Lu, J. Gao, Z.-G. Cui, B. Binks, Effect of trace impurities in triglyceride oils on phase inversion of Pickering emulsions stabilized by CaCO3 nanoparticles, Colloids Surf. A: Physicochem. Eng. Asp. 417 (2013) 126–132.

[48] Z.-G. Cui, K.-Z. Shi, Y.-Z. Cui, B. Binks, Double phase inversion of emulsions stabilized by a mixture of CaCO3 nanoparticles and sodium dodecyl sulphate, Colloids Surf. A: Physicochem. Eng. Asp. 329 (1–2) (2008) 67–74.

[49] M. Destribats, Emulsions stabilisées par des particules colloïdales stimulables: propriétés fondamentales et matériaux, Université Sciences et Technologies-Bordeaux I, 2010.

[50] B.P. Binks, T.S. Horozov, Colloidal particles at liquid interfaces, Cambridge University Press, 2006.